Electron-spectroscopy study of correlation mechanisms in $CuGeO_3$ single crystals

F. Parmigiani
Istituto Nazionale per la Fisica della Materia and Dipartimento di Fisica, Politecnico di Milano, Piazza Leonardo da Vinci, 32-20133 Milano, Italy

L. Sangaletti
Istituto Nazionale per la Fisica della Materia and Dipartimento di Chimica e Fisica per i Materiali, Università di Brescia, Via Branze, 38-25123 Brescia, Italy

A. Goldoni
Laboratorio TASC-INFM, Padriciano 99, I-34012 Trieste and Dipartimento di Fisica, Università di Trieste, Via Valerio 2, I-34127 Trieste, Italy

U. del Pennino
Istituto Nazionale per la Fisica della Materia and Dipartimento di Fisica, Università di Modena, Via Campi 213/A, 41100 Modena, Italy

C. Kim and Z.-X. Shen
Department of Applied Physics and Stanford Synchrotron Radiation Laboratories, Stanford University, 94305-4055 Stanford, California

A. Revcolevschi and G. Dhalènne
Laboratoire de Chimie des Solides, Unité Associée au Centre National de la Recherche Scientifique 446, Université de Paris-Sud, Bâtiment 414, F-91405 Orsay Cédex, France
(Received 10 July 1996; revised manuscript received 2 October 1996)

X-ray (Al-$K\alpha$) and resonant Cu $2p\rightarrow 3d$ and Cu $3p\rightarrow 3d$ photoemission valence-band spectra of high-quality $CuGeO_3$ single crystals are reported and interpreted. In addition, an attempt is given to evaluate the charge transfer (Δ), the $d-d$ Coulomb interaction (U_{dd}) energies, and the superexchange term (J) on the basis of $L_{2,3}M_{4,5}M_{4,5}-L_{2,3}M_{2,3}M_{4,5}$ Auger transitions, and core-level spectra analyzed within the frame of the Anderson Hamiltonian in the impurity limit. The results clearly show that one-electron band-structure calculations do not account for the band gap $\approx$3.7 eV [M. Bassi, P. Camagni, R. Rolli, G. Samoggia, F. Parmigiani, and A. Revcolevschi (unpublished)] and the emission arising from many-body effects (correlated d^8 and d^8-d^9L hybridized states), while Δ and U_{dd}, found to be $\approx$4.2 and $\approx$6.7 eV, respectively, allow us to classify this compound as a charge-transfer insulator with a strong ionic character. In addition, energy-dependent electron-energy-loss measurements suggest that the forbidden d-d intraband transitions are centered at $\approx$1.6 eV, which justifies the blue color of $CuGeO_3$, and the band gap is $\approx$3.7 eV, as required by the transparency of the crystal in the visible region of the electromagnetic spectrum. Finally, in the approximation allowed by the present models, J results to be of the order of -7 meV. [S0163-1829(97)03504-2]

I. INTRODUCTION

$CuGeO_3$ is an inorganic compound that exhibits a spin-Peierls transition at $\approx$14 K (Ref. 1) which implies the presence of strong electron correlation effects. Pure and doped $CuGeO_3$ crystals and powders have been studied in the last two years to investigate the magnetic properties and the origin of the Spin-Peierls phase transition.[2–9] This transition, quite unusual in inorganic compounds, can be viewed as a transition, occurring along the Cu-O chains, from uniform antiferromagnetic (AF) spin-$\frac{1}{2}$ Heisenberg chains to a system of dimerized chains with a singlet ground state. However, a detailed understanding of the electron correlation mechanisms as well as of the electronic and magnetic structure of this compound is needed.

The understanding of electronic excitations in the Cu-O planes is at the center of present-day interests, despite the progress done in the last years. In particular, the local or itinerant character of the carriers in copper-oxide-based compounds and the many-body mechanisms involved in the $d-d$ and $p-d$ charge fluctuations must be addressed. As is well known, high-energy electron spectroscopies are powerful tools to investigate electron correlation mechanisms.[10] Photoemission from the copper core levels can provide important information to evaluate the hybridization term (T_{pd}), the charge transfer energy (Δ), and the $d-d$ Hubbard energy (U_{dd}), while $2p\rightarrow 3d$ and $3p\rightarrow 3d$ valence-band resonance photoemission can probe open d states in one-electron removal spectra of the valence band. The $2p\rightarrow 3d$ and $3p\rightarrow 3d$ resonant spectra in copper-oxide-based compounds have been extensively used to study CuO and related high-temperature superconductors (HTSG's),[10] providing a re-

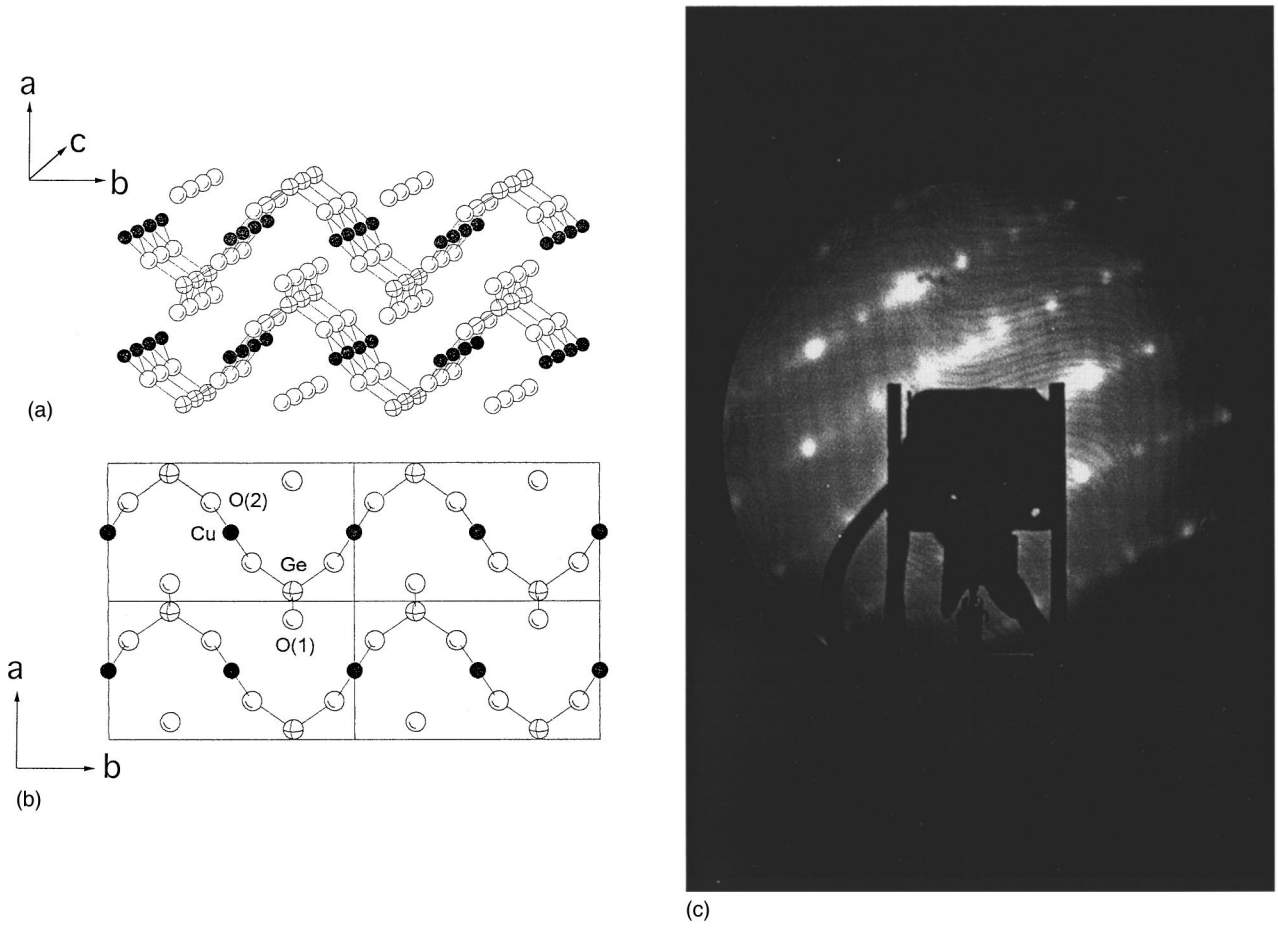

FIG. 1. (a) Crystal structure of $CuGeO_3$. The structure is characterized by chains running along the **c** axis, and of edge-sharing CuO_4 units, where Cu^{+2} ions are at the center of a square of O^{-2} ions. Cu^{2+} ions are also coordinated with two apical oxygen forming an elongated and distorted octahedron (●, Cu; ○, O; ⊕, Ge). (b) View along the *c* axis of the $CuGeO_3$ crystal structure. The nonequivalent oxygen sites are evidenced and labeled as O(1) and O(2). (c) LEED pattern obtained at an electron beam energy of ≈150 eV.

markable fingerprint of the d^8 states versus d^9L and $d^{10}L^2$ (L is the hole in the ligand). The identification of correlated d^8 and d^8-d^9L hybridized states, as well as the magnitude and the nature of the band gap, represent landmark points to be compared with *ab initio* and parametrized band-structure calculations.

The aim of this work is to present and interpret x-ray (Al-$K\alpha$) and resonance valence-band spectra on high-quality $CuGeO_3$ single crystals to probe the correlated d^8 and d^8-d^9L hybridized states. In addition, an attempt is given to evaluate Δ, U_{dd}, the $p-d$ Coulomb interaction (U_{pd}), and the superexchange (J) terms on the basis of $L_{2,3}-M_{4,5}M_{4,5}$ and $L_{2,3}-M_{2,3}M_{4,5}$ Auger transitions and core-level spectra analyzed by the Anderson Hamiltonian in the impurity limit. The results clearly show that one-electron band-structure calculations do not properly describe the band gap (optically determined in Ref. 11) and the emission in the valence band arising from many-body effects, while the charge transfer energy and $d-d$ Coulomb interactions, found to be ≈4.2 and ≈6.7 eV, respectively, allow us to classify this compound as a charge-transfer insulator with a strong ionic character.[12] In addition, energy-dependent electron-energy-loss spectroscopy (EELS) suggests, in agreement with optical data,[11] that the forbidden d-d intraband transitions are centered at ≈1.6 eV, which accounts for the blue color of $CuGeO_3$, and the band gap is ≈3.7 eV, which accounts for the transparency of the crystal in the visible region of the electromagnetic spectrum. These parameters are quite different from those reported in Ref. 13, where an O $2p\rightarrow$Cu $3d$ charge-transfer energy of ≈1.25 eV (identified with the energy gap) and d-d forbidden transitions between ≈2.9 and ≈3.7 eV are suggested. Finally, the superexchange energy, in agreement with calculated values,[14] is found to be ≈7 meV.

II. EXPERIMENT

$CuGeO_3$ crystals are translucent and blue in color and have an orthorhombic cell D_{2h}^5-Pbmm with lattice parameters **a**=4.801 Å, **b**=8.472 Å, and **c**=2.942 Å.[15,16] The crystal structure is characterized by chains of edge-sharing CuO_4 units, where Cu^{+2} ions are at the center of a square of O^{-2} ions, running along the **c** axis. Cu^{2+} ions are also coordinated with two apical oxygen ions, forming an elongated and distorted octahedron. Room-temperature structural measurements[16] show that the Cu-O(1) bond distances [where O(1)

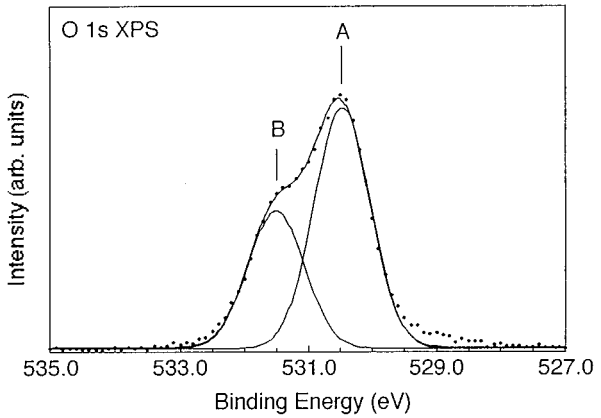

FIG. 2. O 1s core-level emission from $CuGeO_3$. The asymmetry toward the higher binding energy is ascribed to nonequivalent O(1) and O(2) ions. Indeed, this spectral structure can be decomposed into two components centered at ≈530.3 (A) and ≈531.5 eV (B), respectively. The BE of component A, close to those detected in other cuprates (Ref. 19), is attributed to O(2), while line B is attributed to O(1).

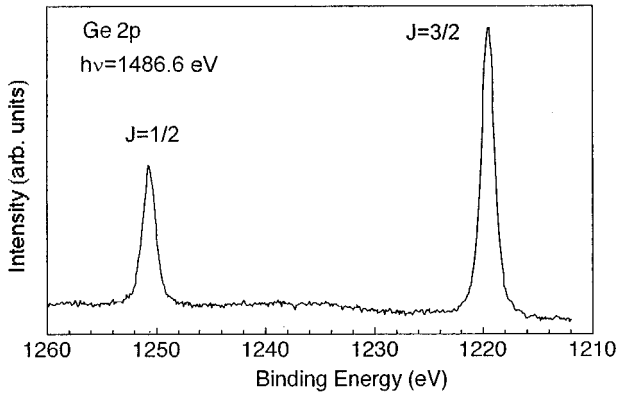

FIG. 3. Ge 2p core-level BE region. The emission at 1219.5 ±0.2 eV is attributed to the Ge $2p_{3/2}$ core level, while the emission at 1250.8±0.2 eV is attributed to the Ge $2p_{1/2}$ core level.

labels the apical oxygen] are d [Cu-O(1)]≈2.77 Å, while the in-plane Cu-O(2) bond distances are d [Cu-O(2)]≈1.94 Å. The chains of edge-sharing CuO_4 units are connected along the c axis by corner sharing units of Ge^{+4} ions tetrahedrally coordinated with O(1) and O(2). The bond-length distances between Ge^{+4} and the oxygen ions are d[Ge-O(1)]≈1.77 Å and d[Ge-O(2)]≈1.72 Å (see Fig. 1).

A high-quality $CuGeO_3$ single-crystal several centimeters long was grown from the melt by a floating zone technique.[17] A piece of this $CuGeO_3$ single crystal with an elliptical section was then oriented on the basis of its Laue pattern, and arranged on a sample holder to be cleaved *in situ* in ultrahigh-vacuum conditions. The samples were easily cleaved perpendicularly to the **a** axis. The exposed **b**-**c** plane resulted in a platelike shaped elliptical surface with major and minor axes 5÷6 mm and $\frac{2}{3}$ mm long, respectively. A low-energy electron-diffraction (LEED) pattern of this surface at room temperature, quite similar to those already reported in the literature,[18] is shown in the inset of Fig. 1.

The samples, obtained from the same single-crystal line rod, were cleaved *in situ*. After cleavage and during the whole set of experiments, the residual pressure in the chambers never exceeded 10^{-10} mbar. X-ray photoemission spectroscopy (XPS) measurements were performed using a Φ mod.5600 electron analyzer. The spectra were collected by irradiating the crystal with a monochromatic Al-$K\alpha$ x-ray source ($h\nu = 1486.6$ eV). The spectrometer was calibrated using the Ag Fermi edge, the Ag $3d_{5/2}$ core level, and the Cu $2p_{3/2}$ core-level to which binding energies (BE's) of 0.0, 368.3, and 932.7 eV were assigned, respectively. The BE scale was then referred to the Ge $2p_{3/2}$ core line, whose maximum was fixed at 1219.5±0.2 eV. By setting the spectrometer pass energy at ≈5 eV, an overall resolution of ≈0.4 eV was obtained for the Ag $3d_{5/2}$ core line. An electron flood gun was used to reduce surface electrostatic charging during the XPS measurements.

The electron-energy-loss spectra were taken in reflection geometry with primary beam energy in the range 200–2000 eV, using the electron gun coaxial to the double-pass cylindrical mirror analyzer. The experimental resolution of 0.5 eV was mainly limited by the energy spread of the electron beam.

Cu $2p \rightarrow$Cu $3d$ resonant photoemission valence-band spectra were collected at undulator beamline 5 at the Stanford Synchrotron Radiation Laboratory. The analytical chamber of this beamline was equipped with a LEED apparatus which was used to perform the room-temperature low-energy electron-diffraction measurements.

III. RESULTS AND DISCUSSION

A. X-ray photoemission core lines

Figure 2 shows the O 1s core-level emission from $CuGeO_3$. An evident asymmetry toward the higher binding energy can be detected. This effect could be the result of the different binding energies for the nonequivalent O(1) and O(2) ions. In fact, this spectral structure can be decomposed in two components centered at ≈530.3 (A) and ≈531.5 eV (B), respectively. The BE of component A, close to those detected in other cuprates,[19] is attributed to O(2), while line B could be attributed to O(1). The relative intensity between components A and B, i.e., ≈2:1, is consistent with this interpretation. As a matter of fact, the Cu ions are connected by an oxygen pair bridge O(2), where the Cu-O-Cu angle is about ≈98°. In turn, this oxygen is bound to Ge ions which should influence the character of the Cu-O(2) bond. It has been recently proposed[14] that the presence of Ge ions attached to bridging oxygen can make the 90° superexchange antiferromagnetic against the Goodenough-Kanamori-Anderson rules. On the other hand, the weak interaction between O(1) and copper ions should be ascribed to the strong Ge-O sp^3 hybrid bond. Therefore, a significant change of the BE and line shape of the O 1s spectra could be expected by substituting Ge ions or modifying the Ge-O bond, and this issue should be addressed in the future.

The Ge 2p core-levels BE region is reported in Fig. 3. Two peaks are clearly detected. Their energy separation and intensity ratio, consistent with the $J = \frac{3}{2}$ and $\frac{1}{2}$ spin-orbit split components, allow us to assign the emission at 1219.5±0.2 eV to the Ge $2p_{3/2}$ core level, while the emission at 1250.8

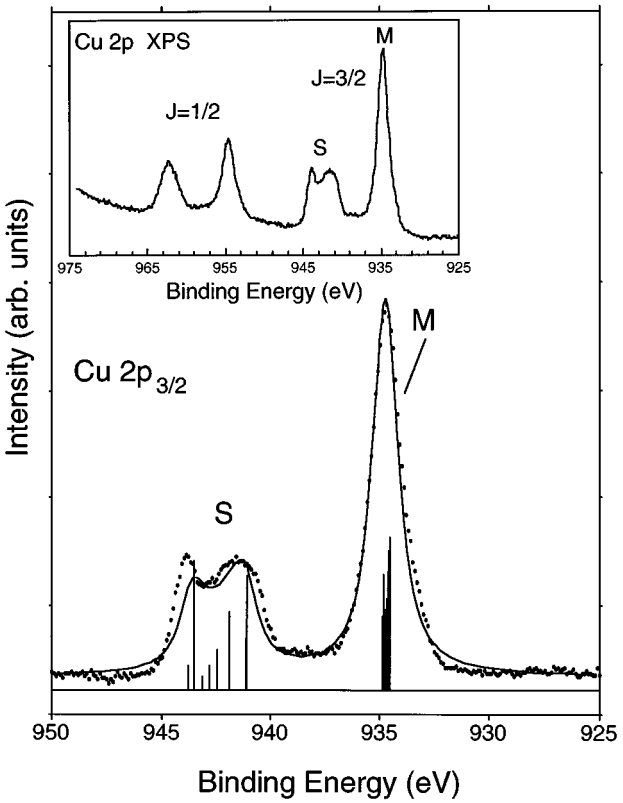

FIG. 4. Cu $2p_{3/2}$ core-level X-ray photoemission spectrum of $CuGeO_3$ (dots). The inset shows the whole Cu $2p$ region. The main line is highly symmetric with an overall full width at half maximum (FWHM) of 1.8 eV. This line has a prevailing Lorentzian character (95 at %). The Gaussian part mimics the instrumental broadening, as well as the oxygen bandwidth contribution to the main line. The Lorentzian contribution, which resulted to be 1.4 eV wide, accounts for the Cu $2p$ core-hole lifetime. The calculated spectrum is represented by a continuous line, and the calculated multiplet structure is indicated by vertical bars with a height proportional to the calculated intensity.

± 0.2 eV is attributed to emission from the Ge $2p_{1/2}$ level. These BE values are consistent with those expected for Ge^{4+} ions.[20]

Figure 4 shows the Cu $2p_{3/2}$ XPS core line. The main line is highly symmetric with an overall full width at half maximum (FWHM) of 1.8 eV. In addition to the main line, a broad satellite, as expected for the Cu^{2+} cuprates, appears in the 940–945-eV binding-energy range. The satellite presents a fine structure, whose origin in other cupric oxides is widely described in the literature,[10,21] arising from multiplet splitting effects due to the interaction between the $2p$ core hole and the $3d^9$ electronic configuration in the final state of the photoemission process.

Although other causes of a double-peak O $1s$ spectrum than different O sites in the structure are known in the photoemission studies on HTSC cuprates (e.g., surface contaminations, different phases at the surface), the Ge $2p$ and the Cu $2p$ spectra are consistent with a sample free of contaminations. In particular, the lack of asymmetry and satellites in the Ge core lines is ascribed to a high-quality cleavage surface. Moreover, a survey spectrum taken at nearly glancing take-off angle indicates that, within the sensitivity of the XPS probe, the surface is free of carbon contaminations.

B. Configuration-interaction approach to the Anderson Hamiltonian in the impurity limit

The analysis of the Cu $2p$ core-level photoemission data was carried out on the basis of the Anderson Hamiltonian model in the impurity limit extended to include exchange and spin-orbit interactions, as described elsewhere.[22] The multiplet splitting for an ionic, unscreened, pd (e.g., $2p3d^9$) configuration was treated according to the interaction scheme proposed by Condon and Shortley[23] and Kotani and Okada.[24,25] The following parameters were used for the exchange and spin-orbit interactions: $F^2(2p,3d)=7.47$ eV, $G^1(2p,3d)=5.62$ eV, $G^3(2p,3d)=3.21$ eV, $\zeta_d=0.13$ eV, and $\zeta_p=13.6$ eV. The eigenvalues, obtained upon the diagonalization of a 12×12 matrix, give the spin-orbit and exchange $Q_{\text{s.o/ex.}}$ contribution to the term Q_{pd} in the final-state Hamiltonian. This accounts for the interaction between the $2p$ core hole and the $3d$ hole in the outer shell. Therefore, the energy Q_{pd} is

$$Q_{pd}^{(i)}=Q+Q_{\text{s.o./exch.}}^{(i)} \quad (i=1,\ldots,12), \tag{1}$$

where Q is the Coulomb part of the two hole pd Slater integral. The intensity ratio l_s/l_m and the energy separation W between the satellite and the main component in the Cu $2p_{3/2}$ spectrum were calculated and compared to the experimental values using a proper extension of the Anderson Hamiltonian in the impurity limit to account for the Q_{pd} multiplet terms of the Cu $2p_{3/2}$ core level. The Δ, T, and Q values representative of $CuGeO_3$ were chosen within parameter sets (with Δ and T ranging from 1.75 to 3.00 eV and Q from 7.5 to 8.5 eV) in order to obtain the best fit between calculated and measured l_s/l_m and W terms. The fit results are shown in Fig. 4, where the continuous line indicates the calculated spectrum. The multiplet lines are also shown below the Cu $2p_{3/2}$ XPS data. The height of each line is proportional to the calculated intensity, while the positions correspond to the calculated binding energies. The peak line shape was obtained assuming a mixture of Lorentzian and Gaussian functions for each calculated line, with a 95 at. % weight of the Lorentzian component. The FWHM of the Lorentzian component is 1.4 eV, while it is 1.175 for the Gaussian component. The dominant Lorentzian component well reproduces the experimental main line, though minor discrepancies at the base of the main line are detectable, likely due to the effect of the oxygen bandwidth (and shape) on the main line. The unusual Gaussian FWHM, which is larger than the expected instrumental broadening ($\sim$450 meV), may also be due to effects arising from the screening of oxygen states in the valence band.

On the basis of this approach, a comparison between CuO, Bi_2CuO_4, and $CuGeO_3$ is rather interesting, since these compounds have CuO_4 units with similar geometry in contrast with the corner-sharing CuO_4 units typical of HTSC cuprates. Table I summarizes the main parameters. Following the arguments of Eskes, Tjeng, and Sawatzky,[26] who showed that the T and Δ values are related to the energy gap, the present results can be interpreted. When going from

TABLE I. Results of the Cl cluster model study. The XPS satellite to main line intensity l_s/l_m ratio; the XPS satellite to main line energy separation, W, the Auger satellite to main line, E_S-E_M; and main line to D peak, E_M-E_D. Energy separations, the calculated T, D, Q_{pd}, U_{dd}, and the nearest-neighbor Cu-O distances are reported. Calculated values for Bi_2CuO_4 and CuO are taken from Ref. 22.

		l_s/l_m	W (eV)	$d_{\text{Cu-O}}$ (Å)	T (eV)	Δ (eV)	Q_{pd} (eV)	E_S-E_M (eV)	E_M-E_D (eV)	U_{pp} (eV)	U_{dd} (eV)
$GeCuO_3$	expt.	0.58	7.59	1.94				4.8	8		
	calc.	0.58	7.57		2.47	4.20	8.55			5.52	6.67
Bi_2CuO_4	expt.	0.53	8.2	1.94				4.8	10		
	calc.	0.535	8.18		2.25	2.8	8.3			5.25	6.55
CuO	expt.	0.46	8.7	1.95				5.0	9		
	calc.	0.47	8.54		2.00	1.75	8.0			4.25	6.5

CuO, to Bi_2CuO_4 and to $CuGeO_3$, Δ and T determined by high-energy core-level spectroscopies increase consistently with the measured energy gaps, being the gap magnitude of Bi_2CuO_4 intermediate between that of the semiconducting CuO and the translucent $CuGeO_3$. Unfortunately, the lack of unambiguous optical data has hindered a quantitative measure of the optical gap of Bi_2CuO_4 and therefore a more solid estimate of Δ. Nevertheless, in the light of the present comparative study, the Δ value of Bi_2CuO_4, based on previous EELS data,[22] has been reconsidered and set to $\approx$2.8 eV. Conversely, the insulating nature of $CuGeO_3$ is confirmed by optical-absorption spectroscopy data,[11] where the onset of the absorption gap is clearly detectable at $\approx$3.7 eV, well above the structures attributed to $d-d$ intra-atomic excitations observed at $\approx$1.8 eV. On the other hand, the Q values, consistently with their origin (intra-atomic Coulomb interaction on the Cu^{+2} sites), are nearly the same for the three compounds under examination.

C. Auger electron spectroscopy

Figure 5 shows the copper $L_{2,3}-MM$ Auger spectrum of $CuGeO_3$ generated by the decay of a photohole in the Cu $2p$ core levels. The spectrum has been divided in two parts corresponding to the regions where the $L_{2,3}-M_{4,5}M_{4,5}$ and $L_{2,3}-M_{2,3}M_{4,5}$ Auger transitions mainly contribute. The assignment of each feature of the spectrum has been done according to literature.[22,27] The most intense peak in each part of the spectrum is the multiplet structure due to the decay of an L_3 photohole when the system is left in the photoemission final state corresponding to the Cu $2p_{3/2}$ main line (see Fig. 4). The spectrum also exhibits distinct and intense Auger satellites, accompanying the main L_3-MM transition, at lower kinetic energies. In an ionic picture these satellites correspond to the Auger transitions $L_3-M_{2,3}3d^8$ and L_3-3d^7. It has been suggested that three processes could contribute to the satellite peaks: (i) the direct Auger decay of an L_3 photo hole when the system is left in the photoemission final state corresponding to the Cu $2p_{3/2}$ satellite; (ii) the Coster-Kronig (CK) decay of an L_2 hole that effectively transfers spectral weight from the L_2-MM Auger transitions to the L_3 satellite regions; and (iii) the CK decay of an L_1 hole. The identification of the contribution of the different decay channels to the Auger satellites, and the analysis of the energy shifts relative to the main L_3-MM transition give information about the correlation energy U_{dd} and the ionicity of the Cu-O bonds.

In order to extract this information, attention was paid to the $L_3-M_{45}M_{45}$ part of the spectrum. The inset of Fig. 5 shows the L_3-3d^8L (M) and L_3-3d^7 (S) Auger transition peaks of $CuGeO_3$. The broad feature above 922 eV (marked D) is the fingerprint of the delocalized two-hole final state in terms of the Cini-Sawatzky model.[28] The relative intensity of feature D compared to the transition arising from the localized two-hole Auger final state M is a function of U_{dd}/BW,[29] where BW is the effective Cu $3d$–O $2p$ hybrid bandwidth. Comparing the Auger spectra of CuO (Ref. 27) and $CuGeO_3$, it is possible to observe that the relative intensity of features M and D is nearly the same, indicating that the ratio U_{dd}/BW is about the same in the two compounds. An estimate of the correlation energy U_{dd} can be obtained considering the energy separation between the localized two-hole final state M ($3d^8L$ final state) and the satellite S ($3d^7$ final state). Neglecting terms arising from the Cu $2p$-hole$\leftrightarrow$O $2p$-

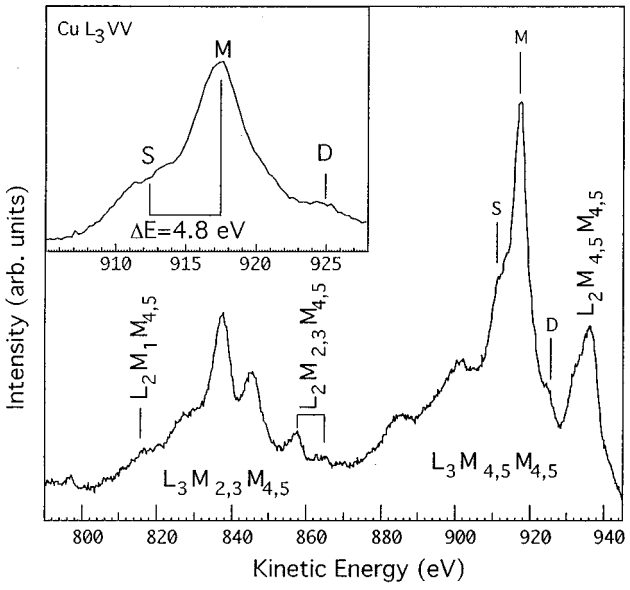

FIG. 5. Copper $L_{2,3}-MM$ Auger spectrum of $CuGeO_3$. The spectrum has been divided into two parts corresponding to the regions where the $L_{2,3}-M_{4,5}M_{4,5}$ and $L_{2,3}-M_{2,3}M_{4,5}$ Auger transitions mainly contribute. The spectrum also exhibits distinct and intense Auger satellites, accompanying the main L_3-MM transition, at lower kinetic energies. In an ionic picture these satellites correspond to the Auger transitions $L_3-M_{2,3}\,3d^8$ and L_3-3d^7.

hole or the Cu $3d$-hole↔O $2p$-hole interactions, the energy separation E_{MS} can be written as

$$E_M - E_S = E(2p^5 3d^{10}L) - E(2p^6 3d^8 L) + E(2p^6 3d^7) - E(2p^5 3d^9) = 2U_{dd} - Q_{pd}. \quad (2)$$

Substituting in Eq. (2) the experimental value of $E_{MS}=4.8$ eV and the calculated value of $Q_{pd}=8.55$ eV, the Hubbard correlation energy U_{dd} results to be ≈ 6.67 eV.

It is also possible to make a rough estimation of the Coulomb interaction U_{pp} in the oxygen $2p$-derived band from the energy difference between the centroid of the delocalized two-hole spectral feature D ($3d^9L^2$ final state) and the energy position of the peak M ($3d^8L$ final state). Their energy separation $E_M - E_D$ can be expressed as $E_M - E_D \approx U_{dd} + U_{pp} - \Delta$. Using the calculated values of $\Delta=4.2$ eV and $U_{dd}\approx 6.67$ eV and the measured values $E_M - E_D \approx 8$ eV and $U_{pp}\approx 5.5$ eV.

D. Magnetic properties

The parameters obtained from the XPS and Auger data analysis can also be used to gain a qualitative understanding of the magnetic properties. For this purpose, the configuration-interaction approach to the Anderson Hamiltonian in the impurity limit was applied to a Cu-O-Cu cluster with the purpose of obtaining an estimate of the superexchange integral J and the Néel temperature. To check the consistency of the model, the calculation was applied also to CuO, Bi_2CuO_4, and $CuGeO_3$.

Magnetic insulators have been treated in the past with the Anderson superexchange theory.[30] It has been shown, however, that when charge-transfer excitations are properly accounted for, better estimates of the Néel temperatures (T_N) for transition metal monoxides are obtained. Indeed, Zaanen and Sawatzky[31,32] proposed, on the basis of the configuration-interaction scheme, the simplest three-center $d_i - L - d_j$ superexchange model including charge-transfer excitations.

In the frame of this model an approximate expression for J is given by

$$J = -2b^2(1/\Delta + 1/U), \quad (3)$$

where $b=T^2/\Delta$, $T=T_e/\sqrt{3}$, and T_e is the e_g transfer integral in the single cation cluster.[30] Expression (3) holds in the case Δ, $T \gg E_0(AF,F)$ and $T^2/\Delta \ll 1$, $T^2/U \ll 1$. As suggested by Sawatzky,[31] the hybridization integral in the present study is further reduced by a factor $\frac{1}{2}$ because only one oxygen between two Cu atoms is involved in the Cu-O-Cu bonding.

Several studies report more sophisticated approaches to the problem of magnetic interactions.[33,34] These calculations are based on a Cu-O bond, geometry where the Cu-O-Cu bond angle is close to 180°, and therefore suitable to treat the case of HTSC's and parent compounds. This is not the case for CuO, Bi_2CuO_4, and $CuGeO_3$, which show Cu-O-Cu bond angles close to 90°. Unfortunately, a model to calculate J in the case of a nonlinear Cu-O-Cu bond is not yet available and in the present work a simpler Cu-O-Cu linear bond is assumed. As a consequence, the calculated J values should be regarded as those resulting from an ''effective'' AF interaction between two Cu^{2+} ions mediated by the presence of O ions. In spite of this rough approximation, the scaling of J's with the parameters obtained from Auger and XPS analysis follows the experimental trend even though the coarseness of the model tends to overestimate J. According to Zaanen,[32] T_N is given by

$$T_N = 2JzS(S+1)/(3k_B n^2), \quad (4)$$

where z is the cation ''magnetic'' coordination number, S the cation spin in the ground state (i.e., $S=1$ for Ni^{2+}, $^3A_{2g}$), k_B the Boltzmann factor, and $n=2S$. The calculation was performed starting from CuO by using the Δ, U_{pp}, and U_{dd} values obtained from the Auger and XPS data analysis, and reducing by a factor 0.81 the hybridization integral T to fit the measured $T_N \approx 220$ K of CuO. J and T_N values of Bi_2CuO_4 and $GeCuO_3$ were then calculated using the appropriate values of Δ, U_{pp}, and U_{dd}, and the same scaling factor (0.81) taken for CuO was applied to the hybridization integrals. The same $z=2$ was used for all the compounds. Table II reports the results obtained solving numerically the Hamiltonian for the Cu-O-Cu cluster.

TABLE II. Calculated antiferromagnetic exchange energies (J) and Néel temperatures (T_N) for CuO, $GeCuO_3$, and Bi_2CuO_4. The t_{pd} parameter was obtained by setting $t_{pd}=0.81T/(2\sqrt{3})$, where T is the hybridization integral reported in Table I.

	CuO	Bi_2CuO_4	$CuGeO_3$
t_{pd} (eV)	0.468	0.528	0.579
J (meV)	19	11.4	6.9
T_N calculated (K)	220	132.5	79.9

The results show a decrease of T_N from CuO to Bi_2CuO_4 and $CuGeO_3$, in agreement with the experiments. However, the calculated absolute values are significantly different from the experimental ones. This discrepancy can be ascribed *in primis* to the improper geometry of the Cu-O-Cu bond used to model the magnetic interactions. However, other factors such as a poor modeling of the antiferromagnetic ordering, which neglects three-dimensional (3D) effects in the coupling of spins on the Cu sites as well as an overestimation of the t_{pd} overlap integrals, should be considered. Indeed, the 3D character of the AF state in Bi_2CuO_4 is supposed to occur via the superexchange coupling of the Cu-O-Bi-O-Cu bond,[35] which, because of its length and the presence of the Bi cation, is likely more screened than in the case of a simple Cu-O-Cu superexchange interaction. The T_N value calculated for Bi_2CuO_4 (≈ 132.5 K) is about three times that experimentally observed [47.5 ± 1.0 K (Ref. 35)]. As for $CuGeO_3$, in which, depending on temperature, a competition between the Spin-Peierls and the AF Néel states occurs, the Cu^{2+} $S=\frac{1}{2}$ spins are strongly coupled in the AF state by intrachain interactions. In this case Poirier *et al.*[4] set the exchange interaction to a typical value of 60 K which is not far from the present value of ≈ 80 K.

E. EELS

As is well known, $CuGeO_3$ has two optical axes along the **b** and **c** crystallographic directions, and polarized beams are required to properly study its optical properties. Electron-

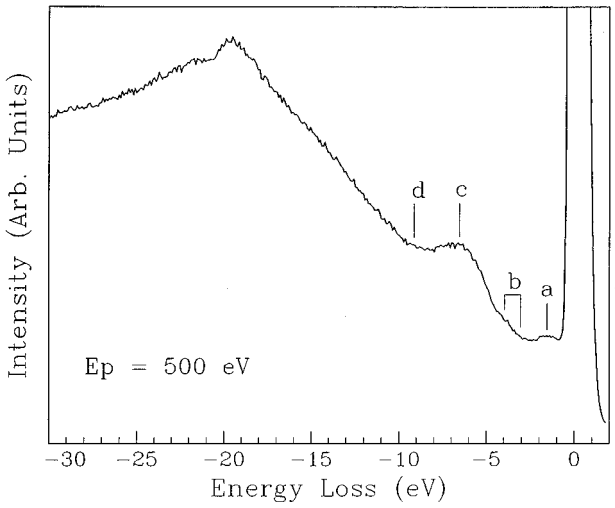

FIG. 6. EEL spectrum of $CuGeO_3$ obtained with a primary beam energy $E_p = 500$ eV. The prominent structures between 25 and 15 eV of the energy loss are assigned to the valence-electron plasmon excitations superimposed to the O $2s \rightarrow$O $2p$ transitions. Below 10 eV, at least four EEL features are detectable at about 1.6 eV (a), 3.0–4.5 eV (b), 6.5 eV (c), and 9.4 eV (d).

energy-loss spectra were obtained using an unpolarized electron beam, therefore the resulting data have a limited quantitative meaning. Nevertheless, some information to support or confirm other measurements can be obtained.

The EEL spectrum of $CuGeO_3$, which we obtained with a primary beam energy $E_p = 500$ eV, is reported in Fig. 6. The prominent structures between energy losses of 15–25 eV are assigned to the valence-electron plasmon excitations superimposed on the O $2s \rightarrow$O $2p$ transitions.[36] More interesting, in the present context, are the features appearing at an energy loss of 10 eV from the quasielastic peak. In this range of losses at least four EEL features are detectable at about 1.6 eV (a), 3.0–4.5 eV (b), 6.5 eV (c), and 9.4 eV (d). The intensities of peaks (b), (c), and (d) do not depend on the electron beam energy,[36] and therefore these excitations are identified as allowed dipole transitions. In particular the lowest of these dipole-allowed transitions [region (b)] corresponds to the Cu $3d \rightarrow$O $2p$ charge-transfer excitations across the electronic band gap. The centroid of this broad feature can be obtained by the second derivative $-dN^2(E)/dE^2$, and its energy position results to be $\approx$3.7 eV. This value is consistent with the charge-transfer energy Δ obtained from Auger and Cu $2p$ core-level data (present paper) and recent optical measurements of the gap.[11] Instead, the excitation at $\approx$1.6 eV (a) exhibits a strong dependence on the primary beam energy E_p [the intensity increases with decreasing E_p (Ref. 36)], indicating that this feature arises from dipole forbidden intraband d-d transitions, in agreement with optical data[11] and against the assignment to charge transfer excitations as stated in Ref. 13.

F. Valence-band photoemission

Band structure calculations on $CuGeO_3$ were carried out by Mattheiss[37] and Popovic, Vikajlovic, and Sljivancanin.[38] As in the case of other late $3d$ metal compounds, standard band methods and the local-density approximation are expected to poorly describe the electronic properties of $GeCuO_3$. Nevertheless, the quite peculiar structure of this compound in which one finds edge-sharing chains of CuO_4 units instead of the more common planes of CuO_4 corner-sharing units such as those found in high-temperature superconducting cuprates, makes the comparison with this last class of materials rather interesting.

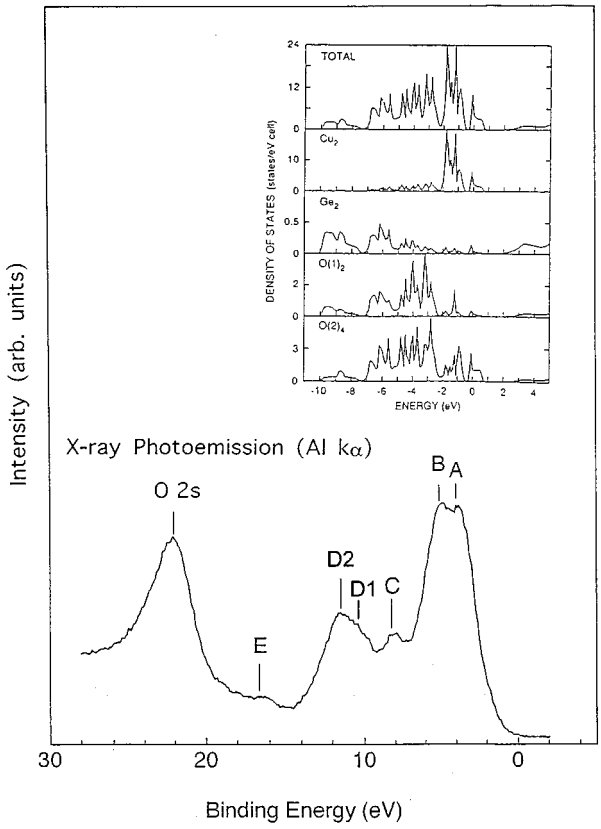

FIG. 7. XPS valence-band spectrum and O $2s$ line of $CuGeO_3$. The O $2s$ contribution is found at 22.5 eV, while a remarkable fine structure can be observed in the 0.0–20.0-eV spectral region. A main and broad structure composed by at least two bands (A and B) is detected at $\approx$4 eV. This dominant emission is followed by a weak but well detectable structure at $\approx$8.5 eV (C). The valence-band spectra is then completed by a rather strong emission at $\approx$12 eV ($D_1 + D_2$) and a weak feature at $\approx$16 eV (E). Inset: calculated DOS in the local density approximation.[37]

The XPS valence-band spectrum and the O $2s$ line of $CuGeO_3$ are shown in Fig. 7. The O $2s$ contribution is found at 22.5 eV, while a remarkable fine structure can be observed in the 0.0–20.0-eV spectral region. A main and broad structure composed by at least two bands (A and B) is detected at $\approx$4 eV. This dominant emission is followed by a weak but well detectable structure at $\approx$8.5 eV (C). The valence-band spectra is then completed by a rather strong emission at $\approx$12 eV ($D_1 + D_2$) and a weak feature at $\approx$16 eV (E). A comparison between these spectra and CuO XPS valence-band spectra[39,40] shows several similarities. Based on the analysis of the character of the eigenstates reported for CuO, emission $A - B$ could be assigned to d^9L final states, while the emission detected between 8 and 14 eV (components $C - D_1 - D_2$) could be assigned to d^8 states with a smaller

contribution of $d^{10}L^2$ states. Even the weak structure detected at ≈16 eV (E) has a counterpart in the CuO XPS spectra, where it has been assigned to a $^1A_1$ state derived from the free-atom ^1S state. Instead, an important difference between the CuO and $CuGeO_3$ valence bands arises if the first ionization state(s) is considered. As is well known, in CuO this state results from the combination of $d^{10}L^2$, d^9L, and d^8 two-hole states, and has an $^1A_{1g}$ symmetry. The two-hole state, which has a wave function

$$|\Psi_{2h}\rangle = \sqrt{0.68}|d_{x^2-y^2}p_{x^2-y^2}\rangle + \sqrt{0.23}|p^2_{x^2-y^2}\rangle + \sqrt{0.09}|d_{x^2-y^2}\rangle,$$

with a dominant $|d_{x^2-y^2}p_{x^2-y^2}\rangle$ character, is the so-called Zhang-Rice (ZR) singlet.[41] In the one-electron valence-band removal spectra of CuO, the ZR singlet is well detected as a steplike structure above the $3d^9L$ main line. In $CuGeO_3$, this feature is not detected, suggesting that the ZR singlet is not stabilized.

Also rather interesting is the comparison between standard band-structure calculations and XPS valence-band one-electron removal spectra. The inset of Fig. 7 reports the density of states of $CuGeO_3$ calculated by Mattheiss.[37] The experimental spectrum and the calculated density of states (DOS) are reported on the same scale. The main differences between calculated and experimental data are those expected when standard band-structure calculations are applied to systems with strong electron correlations. From the calculated DOS, $CuGeO_3$ shows a metallic Fermi edge instead of the ≈3.7-eV band gap observed by optical measurements[11] and EELS. Moreover, the $C-D_1-D_2$ structures observed in the 6–14-eV region of the experimental spectra are completely missing in the calculated DOS, which below ≈8 eV does not show any significant state beside a low intensity contribution originating from Ge and O bands. The fact that standard band calculations fail to predict $C-D_1-D_2$ structures suggests for these features (in agreement with the assignment based on the comparison with CuO) a dominant d^8 character, the emission from this final-state configuration being dominated by significant correlation effects due to the strong Coulomb interaction between the two holes localized on the same copper orbitals. In addition to these main differences, the intensity distribution of the main line is not properly predicted by the calculated DOS.

In order to have a deeper insight into the valence-band structure, resonant photoemission experiments at the Cu $2p-3d$ and Cu $2p-3d$ thresholds were carried out. Resonant photoemission is based on the quantum interference between a direct photoemission, $h\nu + 3d^n \rightarrow 3d^{n-1} + e_k$, where e_k represents the emitted photoelectron and a process such as $(n)p^6 3d^n + h\nu_{(p\rightarrow d)} \rightarrow (n)p^5 3d^{n+1} \rightarrow (n)p^6 3d^{n-1} + e_k$, which arises from a two-electron Koster-Kronig decay of the intermediate state involving an Auger matrix element of the Coulomb interaction. These mechanisms lead to a Fano-like intensity modulation of some valence-band components probing the Cu d^8 final states. As in the case of CuO, the experiment has been performed for the $3p\rightarrow 3d$ ($h\nu \approx 74$ eV) (Refs. 39 and 42) resonant photoemission as well as for the $2p\rightarrow 3d$ giant resonant photoemission ($h\nu \approx 931.5$ eV).[43] The results of the $2p\rightarrow 3d$ giant resonance photoemission for $CuGeO_3$ are reported in Fig. 8. The O $2s$ emission lines

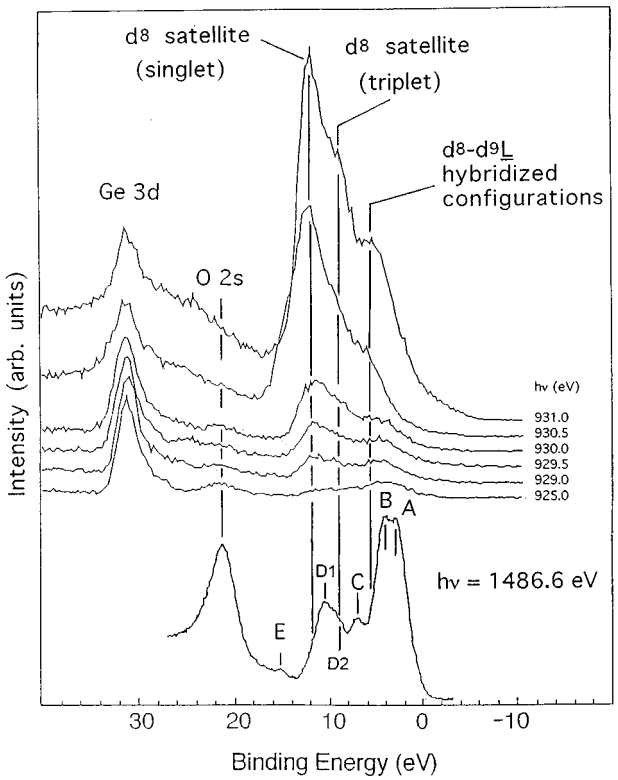

FIG. 8. Resonant photoemission experiments at the Cu $2p-3d$ threshold, with the photon energy $h\nu$ ranging from 925 to 931 eV. The emission lines of the resonant spectra are aligned with respect to the Ge $3d$ core line, while the O $2s$ line of the XPS spectrum is aligned with respect to the O $2s$ emission lines of the resonant spectra. A strong resonance is observed in the 4–14-eV BE region, and three structures can be clearly identified at ≈12, ≈9, and ≈6.8 eV, respectively. Similarly to the case of CuO, the ≈12- and ≈9-eV resonant features are assigned to the d^8 singlet and triplet states, while the ≈6.8-eV structure could originate from d^8-d^9L hybridized configurations.

of the resonant spectra are aligned with the O $2s$ line of the XPS spectrum. A strong resonance is observed in the 4–14-eV BE region and three structures can be clearly identified at ≈12, ≈9, and ≈6.8 eV, respectively. Similarly to the case of CuO, the ≈12 and ≈9-eV resonant features are assigned to the d^8 singlet and triplet states, while the ≈6.8-eV structure could originate from d^8-d^9L hybridized configurations. Therefore, the energy separation between the singlet and triplet states in $CuGeO_3$ is ≈3 eV, respectively, while in CuO it is ≈2.3 eV. Other very important differences between resonant photoemission spectra in CuO and $CuGeO_3$ can be noted: (i) the resonant behavior is extended to the main line; (ii) the singlet state exhibits, as expected, a stronger resonance than the triplet state, but the intensity ratio between these components is smaller than in CuO. Important points to note are also the discrepancies between the BE positions of the $C-D_1-D_2$ features in the XPS valence-band spectrum and the BE of the d^8 singlet and triplet states as well as that of the d^8-d^9L hybridized configurations and the relative extension, in terms of BE, of states with mostly d^8 character. To rationalize, at least qualitatively, this behav-

ior, it is important to consider that the character of the states (d-band occupancy) and their dispersion are in a first approximation determined by the ionicity of the Cu-O bond and by the ratio between the Coulomb interaction energies and the charge-transfer energy. A strongly ionic Cu-O bond will result in a valence band in photoemission spectroscopy with a dominant d^8 occupancy. On the other hand, the separation between d^9L and d^8 states depends on the U_{dd}/Δ ratio. The larger this ratio, the larger the energy separation between d^9L and d^8 states. On the basis of the present analysis the U_{dd}/Δ ratio is $\approx$3.7 for CuO and $\approx$1.6 for $CuGeO_3$. Therefore, in spite of the similarity of the one-electron removal spectra of CuO and $CuGeO_3$, the unusually large distribution of the d^8 states observed in this last compound by resonant photoemission is not surprising. It is also important to note that the BE of the maximum of the resonant features does not coincide with these of structure C and D_2 of the XPS valence band. The direct meaning of this observation is that the maxima of the multiplet split components does not coincide with the singlet d^8 which is found at $\approx$1.5 eV toward the higher BE with respect to component D_2. Instead, the maximum of the triplet states overlaps D_1. Unfortunately, because of the very broad shape of the main resonance, it is very difficult to identify a possible resonance for feature E (attributed to a d^8 singlet state), while feature C remains unexplained considering the maximum of the d^8-d^9L hybridized configurations on the higher BE band edge of the main valence-band structure (between features B and C). Another interesting ''anomaly'' of the resonant photoemission spectra of $CuGeO_3$ arises from the intensity ratio between the d^8 singlet and triplet states. Based on the Auger matrix element for the ^1G states in Cu LVV Auger spectra, the singlets should resonate much more strongly than the triplets. This is not the case for $CuGeO_3$. A possible explanation arises if a relatively large distribution for d^8, the singlet states, is considered. In fact, in this case the intensity of the maximum, in the one electron removal spectra, could not be representative of the overall weight of the d^8 the singlet states. In different terms, the intensity ratio between the d^8 singlet and triplet states should be evaluated from the total weight of these states, and not only from the maximum intensity of their resonating features.

IV. CONCLUSIONS

The results of the present study give a consistent picture of the electronic structure of copper germanate by properly addressing some of the most remarkable electronic and structural properties related to the Cu-O bond in this compound, which ultimately result in the ionic nature of the bond as well as in the spin-Peierls transition at $\approx$14 K.

The electronic correlation parameters of $CuGeO_3$ have been evaluated on the basis of high-energy photoelectron spectroscopy and Auger data. They indicate that $CuGeO_3$ in the ZSA phase diagram is a charge transfer insulator with Δ and $U_{dd}\approx$4.2 and $\approx$6.7 eV, respectively. The Δ value is consistent with the results of optical spectroscopy measurements, and reflects the strongly ionic character of this compound with respect to the HTSC's and related cuprates.

Resonant photoemission measurements of the valence band performed at the Cu $2p\rightarrow$Cu $3d$ absorption edge allowed to probe the d^8 states distribution in the valence-band region, which was found to be quite different from that observed for CuO and HTSC's, suggesting, in agreement with high-energy photoemission spectroscopy data, a larger Δ and a more ionic character of the Cu-O bond in $CuGeO_3$. This information, together with optical and XPS valence-band data, show that standard band-structure calculations are very limited to properly describe the electronic structure of $CuGeO_3$. In particular, they fail to evaluate the gap, the correlated satellites (d^8) and the intensity distribution in the DOS. In addition, it is important to note the absence in the XPS valence band spectrum of structures that can be ascribed to the ZR singlet. This finding addresses a very important issue in the study of hole delocalization in the HTSC in that Cu-O coordination symmetry effects may play an crucial role in driving the electronic features of those bands involved in the transport properties of hole-doped HTSC cuprates.

Finally, EEL data suggest, in agreement with optical measurement, a gap of $\approx$3.7 eV and the presence of dipole-forbidden d-d intraband transitions at $\approx$1.6 eV. These behaviors are responsible for the translucence of $CuGeO_3$ in the visible region of the electromagnetic spectrum and for its blue color.

[1] M. Hase, I. Terasaki, and K. Uchinokura, Phys. Rev. Lett. **70**, 3651 (1993).

[2] B. Roessli, P. Fischer, J. Schefert, W. Bührer, A. Furrer, T. Vogt, G. Petravovskii, and K. Sablina, J. Phys. Condens. Matter **6**, 8469 (1994).

[3] Z. V. Popovic, S. D. Devic, V. N. Popov, G. Dhalenne, and A. Revcolevschi, Phys. Rev. B **52**, 4185 (1995).

[4] M. Poirier, R. Beaudry, M. Castonguay, M. L. Plumer, G. Quirion, F. S. Razavi, A. Revcolevschi, and G. Dhalenne, Phys. Rev. B **52**, R6931 (1995).

[5] M. Nishi, O. Fujita, J. Akimitsu, K. Kakurai, and Y. Fuji, Phys. Rev. B **52**, R6959 (1995).

[6] J. L. García-Muñoz, M. Suaidi, and B. Martínez, Phys. Rev. B **52**, 4288 (1995).

[7] V. Kiryukhin and B. Keimer, Phys. Rev. B **52**, R704 (1995).

[8] H. Takahashi, N. Mori, O. Fujita, J. Akimutsu, and T. Matsumoto, Solid State Commun. **95**, 1995 (817).

[9] R. K. Kremer, Solid State Commun. **96**, 427 (1995).

[10] See, for example, Z.-X. Shen and D. S. Dessau, Phys. Rep. **253**, 1 (1995); W. E. Pickett, Rev. Mod. Phys. **61**, 433 (1989).

[11] M. Bassi, P. Camagni, R. Rolli, G. Samoggia, F. Parmigiani, and A. Revcolevschi (unpublished).

[12] J. Zaanen, G. A. Sawatzky and J. W. Allen, Phys. Rev. Lett. **55**, 418 (1985).

[13] I. Terasaki, R. Itti, N. Koshizuka, M. Hase, I. Tsukada, and K. Uchinokura, Phys. Rev. B **52**, 295 (1995).

[14] W. Geertsma and D. Khomskii, Phys. Rev. B Rapid Commun. (to be published).

[15] G. A. Petrakovskii, K. A. Sablina, A. M. Vorotynov, A. I. Kruglik, A. G. Klimenko, A. D. Balayev, and S. S. Aplesnin, Zh.

Eksp. Teor. Fiz. **98**, 1382 (1990) [Sov. Phys. JETP **71**, 772 (1990)].
[16] H. Völlenkle, A. Wittman, and H. Nowotny, Monatsch Chem. **98**, 1352 (1967).
[17] A. Revcolevschi, and G. Dhalènne, Adv. Mater. **5**, 657 (1993).
[18] C. H. Chen and S.-W. Cheong, Phys. Rev. B **51**, 6777 (1995).
[19] F. Parmigiani, Z.-X. Shen, D. B. Mitzi, I. Lindau, W. E. Spicer, and A. Kapitulnik, Phys. Rev. B **43**, 3085 (1991).
[20] W. E. Morgan and J. R. Van Wazer, J. Phys. Chem. **77**, 96 (1973).
[21] F. Parmigiani and L. Sangaletti, J. Electron Spectrosc. Relat. Phenom. **66**, 223 (1994).
[22] A. Goldoni, U. del Pennino, F. Parmigiani L. Sangaletti, and A. Revcolevschi, Phys. Rev. B **50**, 10 435 (1994).
[23] E. U. Condon and G. H. Shortley, *The Theory of Atomic Spectra* (Cambridge University Press, Cambridge, 1964).
[24] K. Okada and A. Kotani, J. Electron Spectrosc. Relat. Phenom. **52**, 313 (1990).
[25] K. Okada and A. Kotani, J. Phys. Soc. Jpn. **58**, 2578 (1989).
[26] H. Eskes, L. H. Tjeng, and G. A. Sawatzky, Phys. Rev. B **41**, 288 (1990).
[27] S. R. Barman and D. D. Sarma, J. Phys. Condens. Matter **4**, 7607 (1992).
[28] M. Cini, Solid State Commun. **20**, 605 (1976); **24**, 681 (1977).
[29] G. A. Sawatzky, Phys. Rev. Lett. **39**, 504 (1977).
[30] P. W. Anderson, Phys. Rev. **115**, 2 (1959).
[31] G. A. Sawatzky, in *Earlier and Recent Aspects of Superconductivity*, edited by J. G. Bednorz and K. A. Müller (Springer Verlag, Berlin, 1990), pp. 345–376.
[32] J. Zaanen, Ph.D. thesis, University of Groningen, 1986.
[33] H. Eskes and J. H. Jefferson, Phys. Rev. B **48**, 9788 (1993).
[34] M. Kataoka, J. Phys. Soc. Jpn. **62**, 215 (1993).
[35] J. Kostantinovic, G. Stanisic, M. Ain, and G. Parette, J. Phys. Condens. Matter **3**, 381 (1991).
[36] V. Corradini, A. Goldoni, and U. del Pennino (unpublished).
[37] L. F. Mattheiss, Phys. Rev. B **49**, 14 050 (1994).
[38] Z. S. Popovic, F. R. Vikajlovic, and Z. V. Sljivancanin, J. Phys. Condens. Matter **7**, 4549 (1995).
[39] J. Ghijsen, L. H. Tjeng, H. Eskes, G. A. Sawatzky, and R. L. Johnson, Phys. Rev. B **42**, 2268 (1990).
[40] Z.-X. Shen, R. S. List, D. S. Dessau, F. Parmigiani, A. J. Arko, R. Bartlett, B. O. Wells, I. Lindau, and W. E. Spicer, Phys. Rev. B **42**, 8081 (1990).
[41] F. C. Zhang and T. M. Rice, Phys. Rev. B **37**, 3759 (1988); O. Gunnarsson, O. Jepsen, and Z.-X. Shen, *ibid*. **42**, 8707 (1990).
[42] M. L. Thuler, R. L. Benbow, and Z. Hurych, Phys. Rev. B **26**, 669 (1982).
[43] L. H. Tjeng, C. T. Chen, J. Ghijsen, P. Rudolf, and F. Sette, Phys. Rev. Lett. **67**, 501 (1991).